# The nuclear lamina promotes telomere aggregation and centromere peripheral localization during senescence of human mesenchymal stem cells

**Vered Raz[1,2,*], Bart J. Vermolen[3,4], Yuval Garini[4,5], Jos J. M. Onderwater[1], Mieke A. Mommaas-Kienhuis[1], Abraham J. Koster[1], Ian T. Young[4], Hans Tanke[1] and Roeland W. Dirks[1]**

[1]Department of Molecular Cell Biology, Leiden University Medical Center, Leiden, The Netherlands
[2]Department of Human Genetics, Leiden University Medical Center, Leiden, The Netherlands
[3]Biophysical Engineering Group, Faculty of Sciences and Technology, Twente University, 7500 AE Enschede, The Netherlands
[4]Quantitative Imaging Group, Department of Applied Sciences Delft University of Technology, Delft, The Netherlands
[5]Physics Department and Institute of Nanotechnology, Bar-Ilan University, Ramat-Gan 52900, Israel
*Author for correspondence (e-mail: v.raz@lumc.nl)

*Accepted 3 September 2008*
*Journal of Cell Science 121, 4018-4028 Published by The Company of Biologists 2008*
*doi:10.1242/jcs.034876*

## Summary

**Ex vivo, human mesenchymal stem cells (hMSCs) undergo spontaneous cellular senescence after a limited number of cell divisions. Intranuclear structures of the nuclear lamina were formed in senescent hMSCs, which are identified by the presence of Hayflick-senescence-associated factors. Notably, spatial changes in lamina shape were observed before the Hayflick senescence-associated factors, suggesting that the lamina morphology can be used as an early marker to identify senescent cells. Here, we applied quantitative image-processing tools to study the changes in nuclear architecture during cell senescence. We found that centromeres and telomeres colocalised with lamina intranuclear structures, which resulted in a preferred peripheral distribution in senescent cells. In addition, telomere aggregates were progressively formed during cell senescence. Once formed, telomere aggregates showed colocalization with γ-H2AX but not with TERT, suggesting that telomere aggregates are sites of DNA damage. We also show that telomere aggregation is associated with lamina intranuclear structures, and increased telomere binding to lamina proteins is found in cells expressing lamina mutants that lead to increases in lamina intranuclear structures. Moreover, three-dimensional image processing revealed spatial overlap between telomere aggregates and lamina intranuclear structures. Altogether, our data suggest a mechanical link between changes in lamina spatial organization and the formation of telomere aggregates during senescence of hMSCs, which can possibly contribute to changes in nuclear activity during cell senescence.**

Supplementary material available online at
http://jcs.biologists.org/cgi/content/full/121/24/4018/DC1

Key words: Cell senescence, Telomere aggregates, Nuclear lamina, Spatial organization

## Introduction

Marrow stoma cells or mesenchymal stem cells are multipotent, and therefore an important source for the regeneration of damaged tissues and for homeostasis maintenance (Gerson, 1999; Le Blanc and Pittenger, 2005). The relative ease by which they can be isolated and their subsequent manipulation to differentiate into several cell lineages (Pittenger et al., 1999) is a significant advantage for therapeutic use. When grown ex vivo, the division rate of human mesenchymal stem cells (hMSCs) reduces after a few passages, corresponding to cellular senescence and aging (Baxter et al., 2004; Bonab et al., 2006). As the hMSCs exhibit fast cellular senescence without the need for additional manipulations, they can be used as a model system to study the process of cellular senescence.

The process of cellular senescence refers to irreversible growth arrest, which is characterized by quantitative changes in nuclear factors that record the proliferative history of cells, known as Hayflick factors. In human cells, the three best known Hayflick senescence-associated factors are telomere shortening, which results from limited activity and reduced expression of the telomere reverse transcriptase (TERT), accumulation of DNA damage in senescence-associated DNA foci and derepression of the ARF/INK4a locus (reviewed by Collado et al., 2007). Although the general molecular mechanisms underlying the initiation and maintenance of cellular senescence are increasingly recognized, qualitative and quantitative differences are found between organisms and cell types (Ben Porath and Weinberg, 2005; Shay and Wright, 2007; Collado et al., 2007).

Nuclei of senescent cells show significant structural changes, including the formation of the senescence-associated heterochromatic foci (SAHF), which are enriched for several heterochromatin-binding proteins (Narita et al., 2003), the aggregation of the promyelocytic leukemia-nuclear bodies (PML-NBs), which serve as storage hubs for many nuclear proteins (Narita et al., 2003) and the appearance of γH2AX-foci, which are centers for DNA double-strand breaks (Sedelnikova et al., 2004; Cowell et al., 2007). In addition, distorted organization of the nuclear lamina was found in senescent cells (reviewed by Gruenbaum et al., 2005) and in fibroblasts derived from patients carrying mutations in the lamin A gene (Broers et al., 2006; Capell and Collins, 2006). Furthermore, these cells revealed an accumulation of DNA damage and altered histone modifications (Scaffidi and Misteli, 2006), and telomere shortening (Huang et al., 2008), suggesting that changes in lamina organization trigger changes in nuclear function.

A genome-wide study in *Drosophila* revealed that the association of gene clusters with the nuclear lamina changes during development and cell differentiation, and correlates with changes in transcriptional activity (Pickersgill et al., 2006). Studies in various organisms suggest that the nuclear periphery is a zone for transcription repression, although active genes are also found in association with nuclear pores (reviewed by Sexton et al., 2007). Heterochromatic regions, such as telomeres and centromeres are enriched at the nuclear periphery in a cell-cycle-dependent manner (Weierich et al., 2003; Amrichova et al., 2003; Taddei et al., 2004), and recent models suggest that these regions are directly involved in gene repression (Taddei et al., 2004).

An understanding of the process of senescence in hMSCs is important for the successful application of these cells in regenerative medicine. As cellular senescence in hMSCs is not synchronized, we used senescence-associated factors to identify the senescent cells. We applied a lentivirus expression system to express structural nuclear proteins fused to fluorescent probes. As lentiviral DNA is stably integrated into the nuclear DNA of the host cell, these cells do not require any selection pressure by antibiotics, which impose a stress situation. Using newly developed three-dimensional (3D) image processing and image quantification tools, we show that cellular senescence is initially characterized by changes in the vertical axis of the nuclear lamina and followed by changes in the spatial localization of centromeres and telomeres. Significantly, we found that telomeres form aggregates during cellular senescence. Once formed, telomere aggregates are enriched for γ-H2AX but not for TERT. Furthermore, our data revealed binding of telomeres with lamina structures, suggesting that formation of telomere aggregates is a result of association with the lamina. Consistent with this observation, we found that telomeres are also associated with this altered lamina structure and form large aggregates in cells expressing mutant forms of lamin A or lamin B, which exhibit an increase in intranuclear structures of the lamina. We suggest that changes in lamina organization occur during onset of cell senescence and lead to an increase in the association of heterochromatin with the lamina, which is probably characteristic of cell senescence.

## Results

### The lamina structure is spatially deformed in senescent hMSCs

When propagated ex vivo, hMSCs show a slower division rate and reduced differentiation capacity (Pittenger et al., 1999), which is correlated with the appearance of senescence-associated Hayflick factors (Parsch et al., 2004; Zimmermann et al., 2003). As variability in the rate of cellular senescence is found between various donors (Shibata et al., 2007), we first characterized cell senescence in the hMSCs used in this study. Senescent hMSCs showed the hallmarks of cell senescence, accumulation of senescence-associated β-galactosidase (SA-β-gal), formation of γ-H2AX foci and a reduction in TERT expression, and in addition they showed deformation of the nuclear lamina (supplementary material Fig. S1). Using these markers, senescent hMSCs were recognized from passage 7, and at passage 10 the majority of cells showed the hallmarks of senescent cells. We defined the non-senescent cells as 'normal' cells, and used lamina shape to distinguish between normal and senescent cells.

To study the spatial changes of the nuclear lamina during senescence in hMSCs, cells at passage 3 were transduced with a lentiviral vector expressing lamin A-EGFP and, image stacks were collected from living cells using a confocal microscope. 3D reconstructions of cells at passage 4 showed an ellipsoid-like shape of lamin A at the nuclear envelope (Fig. 1A, PS 4). At passage 12, however, most cells showed distortion of the ellipsoid-like nuclear shape and an increase in nuclear depth (Fig. 1A, PS 12). Cross-sections revealed that in senescent cells, lamin A-GFP folds in a vertical direction into the nuclear sphere forming vertical structures that are connected to the lamina at the nuclear envelope. Serial cross-sections suggest that these intranuclear lamina structures protrude into the nucleoplasm in a vertical direction, and in fully senescent cells form a nuclear partition. Interestingly, at passage 6, when cells do not show any senescence-associated features, a distortion of the ellipsoid-like shape was revealed in vertical cross-sections, whereas no aberrations were observed in the horizontal plane (Fig. 1A, PS 6). This analysis suggests that changes of lamina organization are an early feature of cellular senescence. Furthermore, our analysis indicates that distortion of the lamina structure increases during cell senescence, where formation of vertical structures precedes changes in the horizontal plane.

The changes in nuclear shape, observed by confocal microscopy were analyzed under higher magnification using electron microscopy (EM). At passage 9, we recognized cells with a smooth ellipsoid shape of the nuclear envelope and cells with intranuclear membrane structures (Fig. 1Bi and ii, respectively). Interestingly, some changes in the structure of chromatin close to the nuclear envelope were recognizable in cells with intranuclear membrane structures. Vertical sections of the cells revealed that in cells with an ellipse-shaped nucleus, a regular organization of condensed chromatin was present close to the nuclear envelope (Fig. 1Biii), whereas in senescent cells, the organization of chromatin close to nuclear envelope appeared less uniform (Fig. 1Biv). As the interaction between the nuclear lamina and chromatin is dramatically changed during cell differentiation and development (Pickersgill et al., 2006), we investigated whether changes in the spatial organization of centromeres and telomeres, also correlate with changes in lamina organization during cell senescence.

### Centromere localization shifts to the nuclear periphery in senescent hMSCs

Previous studies showed that centromeres obtain a more peripheral localization in cell-cycle-arrested cells and in differentiated cells (Cremer et al., 2004). More recently, we made a similar observation in cells that were targeted for apoptosis (Raz et al., 2006). We wondered whether a similar redistribution of centromeres would take place during cell senescence. Therefore, we analyzed the spatial distribution of centromeres in relation to the nuclear lamina in hMSCs expressing CenpA-GFP (Sugimoto et al., 2000) and lamin-A-DsRed. Confocal images were taken of live cells, and 3D reconstructions were made from the collected Z-stacks (Fig. 2Ai). The spatial distribution of CenpA-GFP was analyzed in nuclei segmented on lamin-A staining. This method enabled us to detect changes in centromere localization in relation to the nuclear sphere (Vermolen et al., 2008). Quantification of pooled data revealed a relocalization of centromeres toward the nuclear periphery in hMSCs at passage 12 compared with their localization in cells at passage 6 (Fig. 2Aii). The *P* value from the Kolmogorov-Smirnov Test (KS test) indicates that this change in distribution is significant. Our observations here are consistent with previous studies showing that a preferred peripheral nuclear localization of centromeres is found in G0 and G1 arrested cells (Gilchrist et al., 2004; Solovei et al., 2004).

This preferred peripheral distribution of centromeres can be a result of the increase in nuclear depth or due to changes in lamina

organization in senescent cells. To test whether the redistribution of centromeres in senescent cells correspond to spatial changes in lamina organization, we analyzed the fluorescence intensity plots of cross-sections in the *x*-*z* and *y*-*z* axis of confocal images (Fig. 2Bi). In cells at passage 6, 12% of the centromeres colocalized with the lamina, whereas at passage 12, this percentage increased to 38% (Fig. 2Bii). These results suggest that centromere localization at the nuclear periphery in senescent cells could be driven by the lamina.

### Telomeres form aggregates in senescent hMSCs

Because senescence correlates with telomere shortening in hMSCs (Baxter et al., 2004; Bonab et al., 2006; Stenderup et al., 2003), we investigated whether the spatial organization of telomeres is also changed in senescent cells. hMSCs at passage 3 and 12 were hybridized with a peptide-nucleic acid (PNA) probe that binds to the telomeric repeat sequence (Molenaar et al., 2003), and confocal 3D images were taken for quantitative analysis of telomeres. Maximum projections revealed a mix of large and small PNA fluorescent dots in cells at passage 12, whereas at passage 3, only small dots were observed (Fig. 3A). After plotting intensity values of the PNA fluorescent dots, a difference in telomere organization became apparent between cells at passage 3 and passage 12 (Fig. 3Aii). We previously showed that an increase in fluorescence intensity corresponds to the formation of telomere aggregates (Raz et al., 2006). To better characterize the spatial reorganization of telomeres during cell senescence, telomere aggregates were mathematically defined with the thresholds *t* and *T* (see Materials and Methods). The outliers above the *T* threshold indicate big telomere aggregates and the outliers between the thresholds *T* and *t* indicate small aggregates (Fig. 3Aii). Few small telomere aggregates ($t<i<T$) were found in cells at early and late passages, but large aggregates ($i>T$) were found only in cells at passage 12 (Fig. 3Aii,iii). A quantitative comparison revealed that the ratio between fluorescence intensity in aggregates and total telomere fluorescence intensity as well as the percentage of telomeres that are found in aggregates increased between passage 3 and 12 (Fig. 3Aiv). Notably, among cells at passage 12 we found cells that contained mainly large PNA fluorescent dots and only a few small ones (Fig. 3Aic). We conclude that telomeres progressively aggregate during cellular senescence.

We next asked whether the formation of telomere aggregates correspond to changes in the lamina. PNA hybridization was combined with lamin A immunofluorescence on cells at passage 9. The deformed nuclear shape and the increase in nuclear depth were used as markers to sort between senescent and normal cells in the mixed cell population found at passage 9 (Fig. 3Bi). Statistical analyses revealed a clear correlation between telomere aggregate formation and the deformed nuclear shape (Fig. 3Bii), suggesting a correlation between changes in lamina shape and the formation of telomere aggregates.

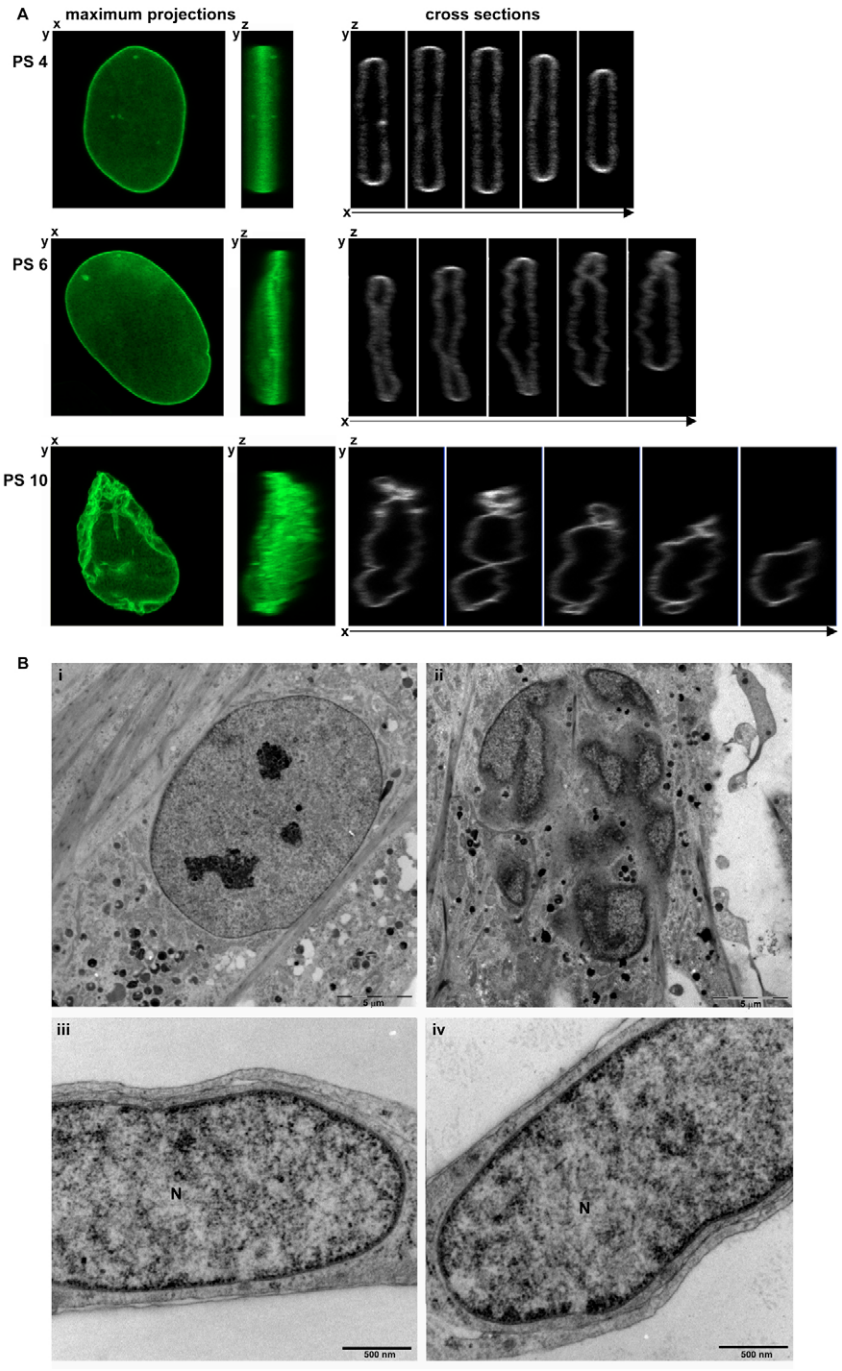


**Fig. 1.** Spatial changes in lamina organization during cellular senescence in hMSCs. Changes in the spatial organization of lamin A during senescence of hMSCs. Cells at passage 3 were transduced with the lamin A-EGFP lentiviral vector and cultured for 9 passages. (A) Confocal images were taken from living cells at passage 4, 6, and 12 (PS 4, PS 6 and PS 12, respectively). Maximum projections of *x*-*y* and *y*-*z* axes from representative nuclei (left). Cross-sections 55 nm deep were made from the *y*-*z* axis. Shown are five serial sections at equal intervals (right). (B) Electron microscope images of horizontal (i,ii) or vertical (iii,iv) sections of hMSCs at passage 9, taken from normal (i,iii) or senescent cells (ii,iv). N, nucleus.

### hMSCs obtained from an old donor show senescence-associated changes in nuclear architecture

We have examined the changes in the spatial organization of lamina, telomeres and centromeres in senescent hMSCs isolated from a 35-year-old individual. To validate the changes in centromere and telomere spatial organization during cell senescence, we compared nuclear organization between cells of two donors aged 35 and 81 years. The expression levels of the Hayflick senescence-associated factors, p16(INK4a) and TERT, as well as SA-β-Gal staining and reorganization of PML-NBs, all indicate rapid cellular senescence of cells from the 81-year-old donor (81y cells) (supplementary material Fig. S2). Although we compared cells from two donors only, our observations confirm previous studies showing that hMSCs isolated from old donors senesce faster in vitro compared with those isolated from younger donors (Stenderup et al., 2003; Baxter et al., 2004). The faster senescence of the 81y cells was found to be associated with the formation of telomere aggregates and redistribution of telomeres and centromeres to the nuclear periphery. The spatial organization of telomeres was studied in living cells expressing TRF1-DsRed and lamin B-EGFP at passage 7 (Fig. 4Ai). Most of the 35y cells exhibited a normal morphology, whereas the 81y cells accumulated senescence-associated markers. After quantification of the TRF1 fluorescent dots, a two- to fourfold increase in telomere aggregates was found in 81y cells compared with that found in 35y cells (Fig. 4Aii). Notably, only small telomere aggregates were found in the 35y cells, whereas large telomere aggregates formed in the 81y cells (Fig. 4Aii). Thus, cell senescence in the 81y cells is correlated with the formation of telomere aggregates. The spatial distribution of telomeres and centromeres from the center of mass was studied with CDF plots, which revealed a preferred peripheral localization of both TRF1 and CenpA in the 81y cells compared with that in 35y cells (Fig. 4Aiii; Fig. 4B, respectively). This difference in localization between the 81y and 35y cells is statistically significant (Fig. 4Aiii; Fig. 4B). Thus, during cell senescence in hMSCs, telomeres form aggregates and shift to a peripheral localization, suggesting that change in telomere organization is associated with changes in lamina organization.

### Telomere aggregates have characteristics of damaged telomeres and lack TERT

We next asked how telomeres in aggregates differ from individual telomeres. Although normal telomeres are associated with TERT, damaged telomeres do not colocalize with TERT but contain DNA damage γ-H2AX foci (Seldelnikova et al., 2004). A spatial overlap between TRF2 and TERT was analyzed in the 81y cells at passage 7, expressing TRF2-citrine and lamin A-DsRed, which was used to discriminate between senescent and normal cells. Fluorescence intensity plots revealed a significant amount of overlap between TRF2 and TERT in cells exhibiting the normal ellipsoid lamin A shape (Fig. 5Ai, right panel, white arrows). In cells showing a deformed lamina shape, TERT did not overlap with telomere aggregates (gray arrows), but only with individual telomeres (white arrows) (Fig. 5Aii). In cells showing an extreme deformation of the lamina structure and reduced TERT expression, TERT did not localize at individual telomeres (Fig. 5Aiii). Interestingly, we observed that the staining pattern of TERT and lamin A overlapped to some extent in senescent cells (Fig. 5Bi, merge). This overlap between lamin A and TERT localization was confirmed by a quantitative analysis of Z-stacks. In non-senescent cells, showing a normal lamina shape, TERT is localized throughout the nucleoplasm and at elevated levels in nucleoli (Fig. 5Bii), which is in agreement with the localization of TERT in differentiated cells (Yan, 2004). Furthermore, some colocalization of TERT with lamin A was observed at the nuclear rim (Fig. 5Bii). A more pronounced

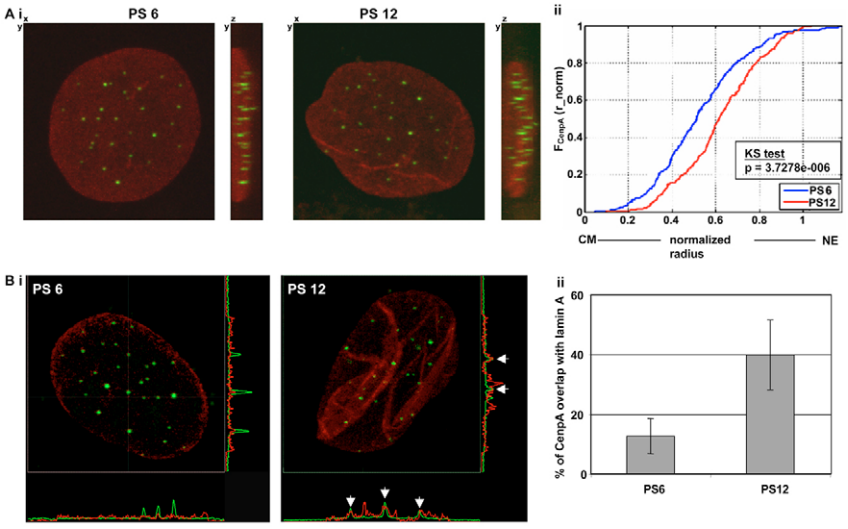


**Fig. 2.** Centromeres shift to peripheral localization in cellular senescent hMSCs. Cells at passage 3 or 9 were transduced with the CenpA-EGFP (green) and the Lamin A-DsRed (red) lentiviral vectors, and imaging was carried out on cells at passages 6 and 12. (A) Maximum projections of cells at passage 6 or 12 on the *x-y* and *y-z* axis. The spatial localization of centromeres was obtained from cells at passage 6 and 12. CDF plots of centromere spatial localization are shown (right). CDF plots show the normalized frequency as a function of a normalized nucleus radius. Statistics show pooled data taken from 12 cells per passage. The Kolmogorov-Smirnov Test (KS Test) *P* value is indicated and suggests that the underlying distributions differ significantly. (B) Quantification of spatial overlap between CenpA and lamin A. Images of CenpA-EGFP and lamina-DsRed were taken from hMSCs as described in A. Quantitative overlap fluorescence intensities between CenpA and lamina A were spatially analyzed in cross-sections. Maximum projections (*x-y* axis) of lamin A-DsRed (red) and CenpA-EGFP (green) in a representative cell at passage 6 or passage 12. Fluorescence intensities of both probes are plotted in the *y-z* or *x-z* axes (graphs below and to right of confocal images). The spatial overlap between lamin A and CenpA is indicated by arrows. Histograms show the percentage of CenpA overlapping with lamin A, in cells at passage 6 and 12. Results are mean ± s.d. of ten cells.

overlap between TERT and lamin A was observed in senescent cells at intranuclear structures (Fig. 5Biii). This suggests that TERT is retained at the intranuclear lamina structure, thereby reducing its availability at telomeres.

We next investigated whether telomere aggregates share characteristics of DNA damage foci and colocalize with γ-H2AX. The extent of colocalization between telomere aggregates and γ-H2AX foci was studied in cross-sections of confocal images taken from the 81y cells at passage 7. In cells with an ellipsoid lamina shape only 11% of the TRF1-fluorescent dots, which correspond to individual telomeres, overlapped with γ-H2AX foci. This percentage of overlap between telomeres and γ-H2AX foci is in agreement with previous reports (Seldelnikova et al., 2004). However, when telomere aggregates were identified, only 37.5% of the telomere aggregates overlapped with γ-H2AX foci (Fig. 5Cii, indicated with an arrow). Importantly, in cells showing an extensive distortion of lamin A and mainly large telomere aggregates, nearly all telomere aggregates overlapped with γ-H2AX foci (Fig. 5Ciii).

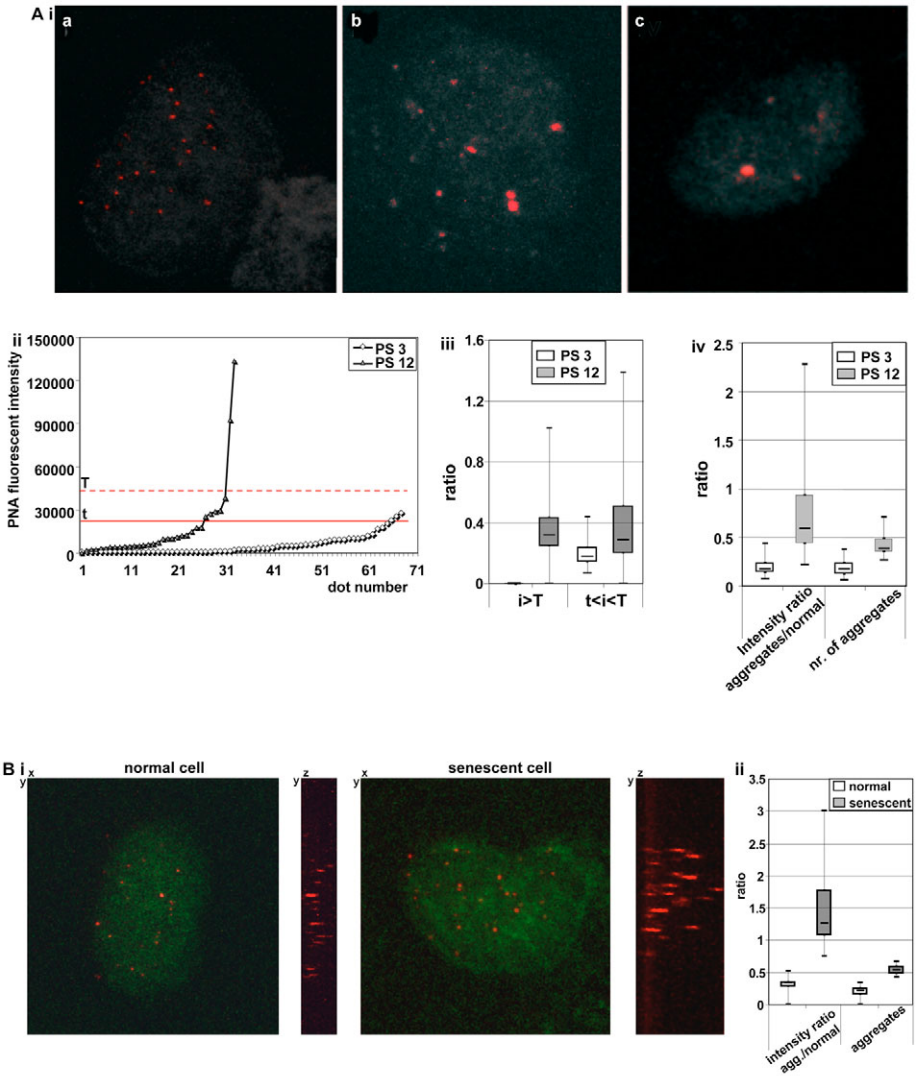


**Fig. 3.** Telomeres form aggregates during cellular senescence in hMSCs. (A) Telomeres form aggregates in cells at passage 12. Cells at passage 3 and 12 were labeled with PNA probes to identify telomeres. 3D image processing and quantitative image analysis of PNA fluorescence was carried out using TeloView. (Ai) Maximum projections of PNA hybridization from representative nuclei at passage 3 (a) and 12 (b and c). A nucleus with mainly telomere aggregates (c) represents a class of cells found at passage 12, which were excluded from statistical analyses. (Aii) Telomere fluorescence intensity in cells at passage 3 and 12. The PNA fluorescent dots were sorted and plotted according to their intensity. Shown are the intensity plots obtained from a typical cell in passage 3 (open squares) and 12 (closed triangles). The thresholds for definition of small and big telomere aggregates are indicated with straight or dashed red lines, respectively. (Aiii) B-box plots of the ratio of big telomere intensities (i>T) or small telomere intensities (t<i<T) to all telomeres in cells at passage 3 and passage 12. (Aiv) B-box plots of the ratio in the fluorescent intensity between telomere aggregates (i>t) (agg.) to normal telomeres, and the ratio between the number of spots found in aggregates to total PNA spots. Statistical analyses represent 1400 PNA fluorescent dots obtained from 20 cells per passage. Based on fluorescence intensity, the PNA fluorescent dots are calculated as equivalent to 90-100% of expected telomeres. Cells with less telomeres (Fig. 2Aic) were excluded from statistical analyses. (B) Telomere organization correlates with changes in nuclear shape. hMSCs at PS 9 were labeled with PNA followed by immunofluorescence with anti lamin B antibody (visualized in green). 3D reconstructions of confocal images were carried out using Teloview. Based on lamin B organization and the nuclear depth, cells were grouped into normal and senescent groups. Maximum projections of the *x*-*y* and *y*-*z* axis show representative normal or senescent cells B-box plots on the right show the ratio in the fluorescent intensity between telomere aggregates (i>t) (agg.) to normal telomeres, and the ratio between the number of spots found in aggregates and total PNA spots. Statistical analysis involved 1050 PNA fluorescent dots obtained from 15 cells per group.

These results in hMSCs confirm previous studies in immortalized cells where telomere localization overlaps with γ-H2AX foci after induction of cellular senescence (Takai et al., 2003; Seldelnikova et al., 2004). In addition, our data revealed overlap between γ-H2AX DNA foci and telomere aggregates, but not with individual telomeres, suggesting that once formed, telomere aggregates are associated with γ-H2AX DNA foci.

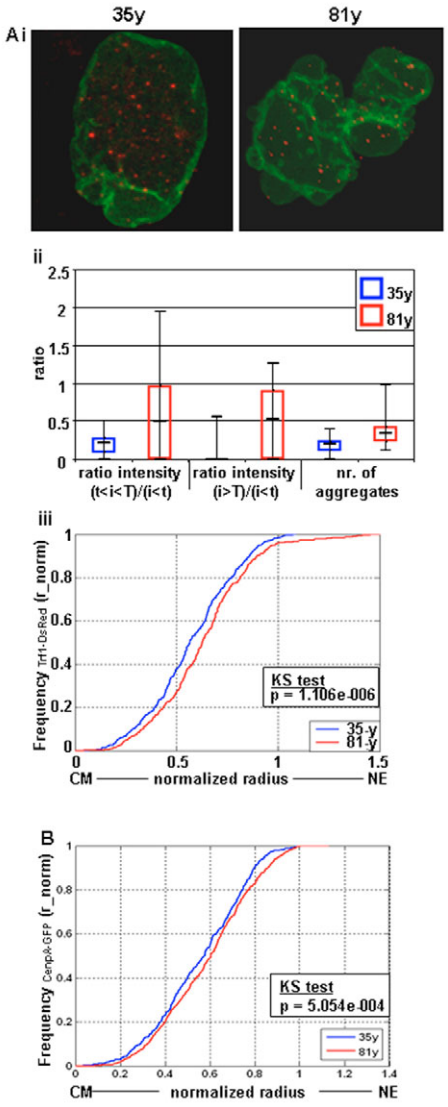


**Fig. 4.** Comparison of telomere and centromere spatial organization in 35y and 81y hMSCs. The 35y and 81y cells were isolated from two individuals at age 35 (35y) and 81 (81y). (A) Formation of telomere aggregates in 81y cells at passage 6. Cells at passage 5 were transduced with TRF1-DsRed lentiviral vectors. 3D B-box plots show the ratio in the fluorescent intensity between small telomere aggregates and normal telomeres [$(t<i<T)/(i<t)$], the ratio in fluorescent intensity between large telomere aggregates and normal telomeres [$(i>T)/(i<t)$] and the ratio between the number of dots found in aggregates to total TRF1 fluorescent dots. CDF plots (bottom left) show the normalized frequency as a function of a normalized nucleus radius. The *P* value (KS Test) is indicated and suggests that the underlying distributions differ significantly. Statistical analyses represent 1750 TRF1-DsRed fluorescent dots obtained from 25 cells per cell class. (B) CDF plots of CenpA spatial localization in 35y and 81y cells. Cells at passage 5 were transduced with CenpA-EGFP lentivirus vectors. Confocal images were taken from living cells at passage 6. The plots show the normalized frequency as a function of a normalized nucleus radius. The *P* value (KS Test) is indicated and suggests that the underlying distributions differ significantly. Statistical analyses represent 525 CenpA-fluorescent dots obtained from 15 cells per cell class.

### Increased telomere association with the lamina correlates with the formation of telomere aggregates

Our results so far, suggest a correlation between changes lamina structure and the formation of telomere aggregates. Therefore, we next examined whether changes in lamina structure affect telomere binding to the lamina. Binding of telomeres to the lamina proteins was studied using chromatin immunoprecipitation followed by a quantitative PCR (ChIP-QPCR) with telomere-specific primers (Cawthon, 2002). Specific binding of telomeres to lamin A or lamin B was found in U2OS cells expressing lamin-A-GFP or lamin-B-GFP (Fig. 6A). Cells expressing CMV-GFP showed only a background level of PCR products, whereas elevated telomere PCR products were seen in cells expressing TRF1-Citrine (Fig. 6A). These results are consistent with previous data revealing limited telomere binding to the nuclear lamina structure in immortalized cells (Luderus et al., 1996). Furthermore, the quantitative analysis indicates that telomere binding to lamin A is preferred over binding to lamin B. These results are consistent with in vitro data showing that lamin B binds less efficiently to telomere-repeat sequences than lamin A or lamin C (Shoeman and Traub, 1990).

We next applied the ChIP-QPCR method to hMSCs to investigate whether an increase in nuclear lamina folding may lead to an increase in binding of telomeres to the lamina proteins. Mutant forms of lamin A and lamin B proteins were expressed in hMSCs to induce the formation of lamina intranuclear structures (Fig. 6D). The lamin A-R133L mutation is a dominant mutation found in patients with Werner's syndrome, which affects the structure of the lamina (Jacob et al., 2005). The lamin A-R220Q dominant mutation is localized at the variable linker L12, which connects the 1B and 2A α-helical segments found in various laminopathies (Dhe-Paganon et al., 2002; Broers et al., 2006). Mutations in L12 affect the structure of the nuclear lamina (Strelkov et al., 2003). The L158D mutation in lamin B creates an additional caspase-3 site. This is a gain-of-function mutation that leads to a severely deformed structure of the nuclear lamina (Raz et al., 2006). Expression of these lamin mutants in hMSCs led to changes in lamina structure and the formation of lamina intranuclear structures by passage 5 (Fig. 6C). In addition, enhanced association of telomeric repeats with lamina proteins was found in cells expressing these mutants. Expression of the lamin-A R133L or lamin-A R220Q mutants resulted in a 2.5- to 4-fold increase in telomere binding compared with WT lamin A, as revealed by ChIP analysis (Fig. 6B). Interestingly, expression of the lamin B mutant showed a 16-fold enrichment in telomere binding compared with binding to WT lamin B (Fig. 6B). Together these results suggest that an increase in lamina folding leads to an increase in telomere binding to the lamina.

We then tested whether changes in lamina structure lead to the formation of telomere aggregates in these lamin mutants. Cells expressing the lamina mutants were co-transduced with TRF1-DsRed lentiviral vectors (Fig. 6C) and telomere organization was studied in representative cells by confocal microscopy. Telomere aggregates were recognized in the intensity plot of TRF1-DsRed. Telomere aggregates were detected in cells expressing lamin A R133L-EGFP, lamin A R220Q-EGFP or lamin B L158D-EGFP mutations, but not in cells expressing WT lamin-A-EGFP (Fig. 6D). Significantly, the formation of telomere aggregates was more pronounced in cells expressing lamin-B L158D-EGFP compared with cells expressing the lamin A mutants. These results suggest a

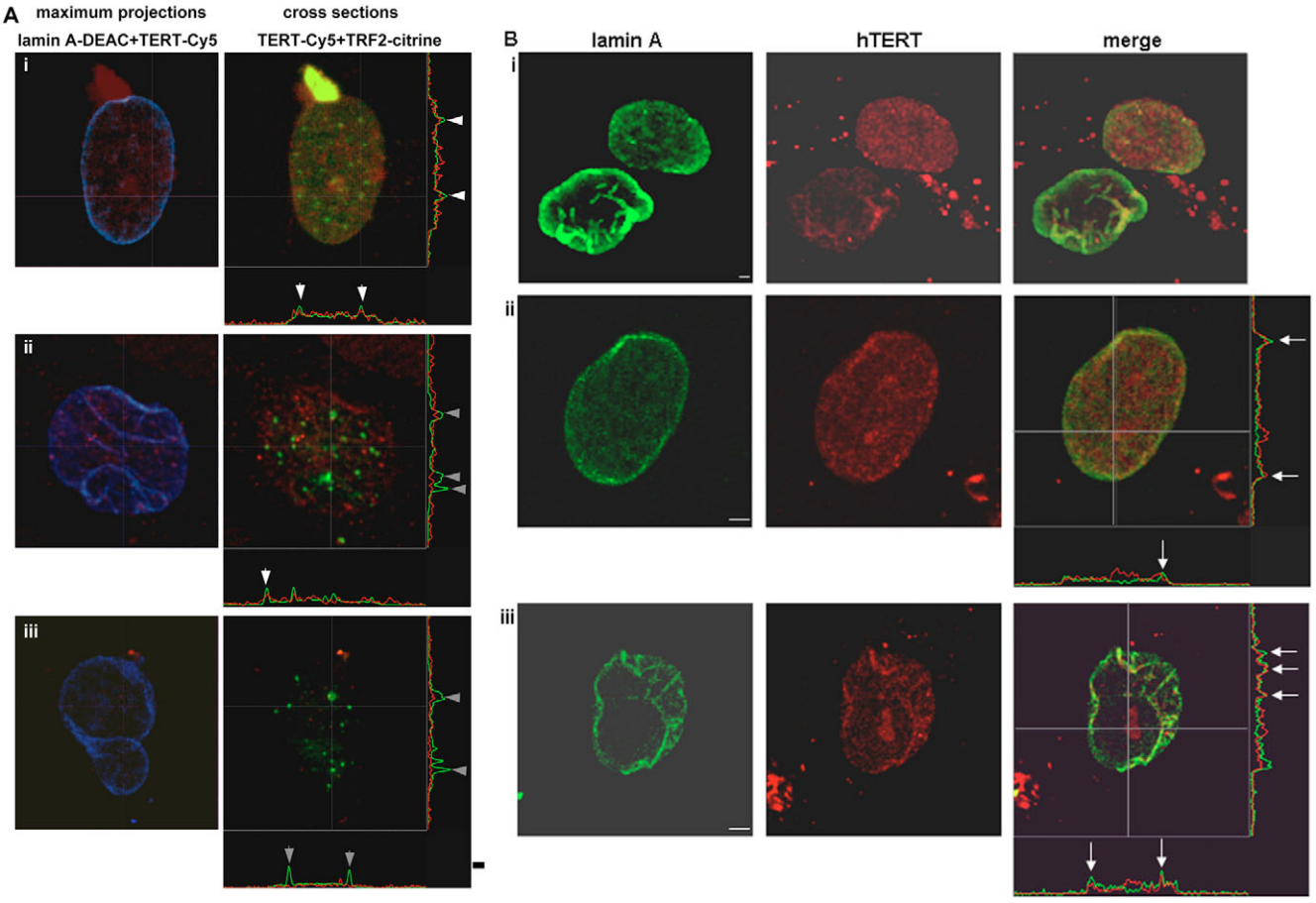


**Fig. 5.** Telomere aggregates are associated with γ-H2AX foci but not with TERT. (A) Telomere aggregates do not overlap with TERT in senescent cells. The 81y cells were transduced at passage 6 with Trf2-citrine lentiviral vector, and immunodetection with anti-TERT and anti-lamin-A antibodies was carried out on cells at passage 7. Left panels show maximum projections of TERT (red) and lamin A (blue) in normal (i) or senescent (ii,iii) cells. Right panels show maximum projections of TRF2 and TERT in the *x-y* axis. Fluorescence intensity graphs on the *y-z* or *x-z* axis show overlap in distribution (indicated with white arrows). Gray arrows indicate large TRF2 aggregates. (B) TERT colocalizes with intranuclear structures of the lamina in senescent hMSCs. Immunofluorescence with anti-TERT (green) and anti-lamin A (red) antibodies was carried out on hMSCs at passage 9. (i) Wide-field fluorescence microscope images show a correlation between lamina deformed shape and reduced expression level of TERT in senescent cells. Scale bars are equal 15 μm. (ii,iii) Cross-sections (*x-y* axis) of confocal images show a cell with a normal ellipse lamina structure (ii) or a distorted lamina shape (iii). The overlap in spatial localization between lamin A (red) and TERT (green) is indicated in the intensity plots in the merged images. (C) Large telomere aggregates overlap with γ-H2AX in cells with a folded lamina structure. The 81y cells were transduced at passage 6 with TRF1-citrine followed by transduction with lamin A. At passage 7, cells were immunolabeled with anti γ-H2AX antibody. Left panel shows merged images of lamin A-EGFP (blue) and TRF1-citrine (yellow), middle panel shows merged images of lamin A-EGFP (blue) and γ-H2AX (red), and right panel shows merged images of TRF1-citrine (yellow) and γ-H2AX (red) in normal (i) or senescent (ii,iii) cells.

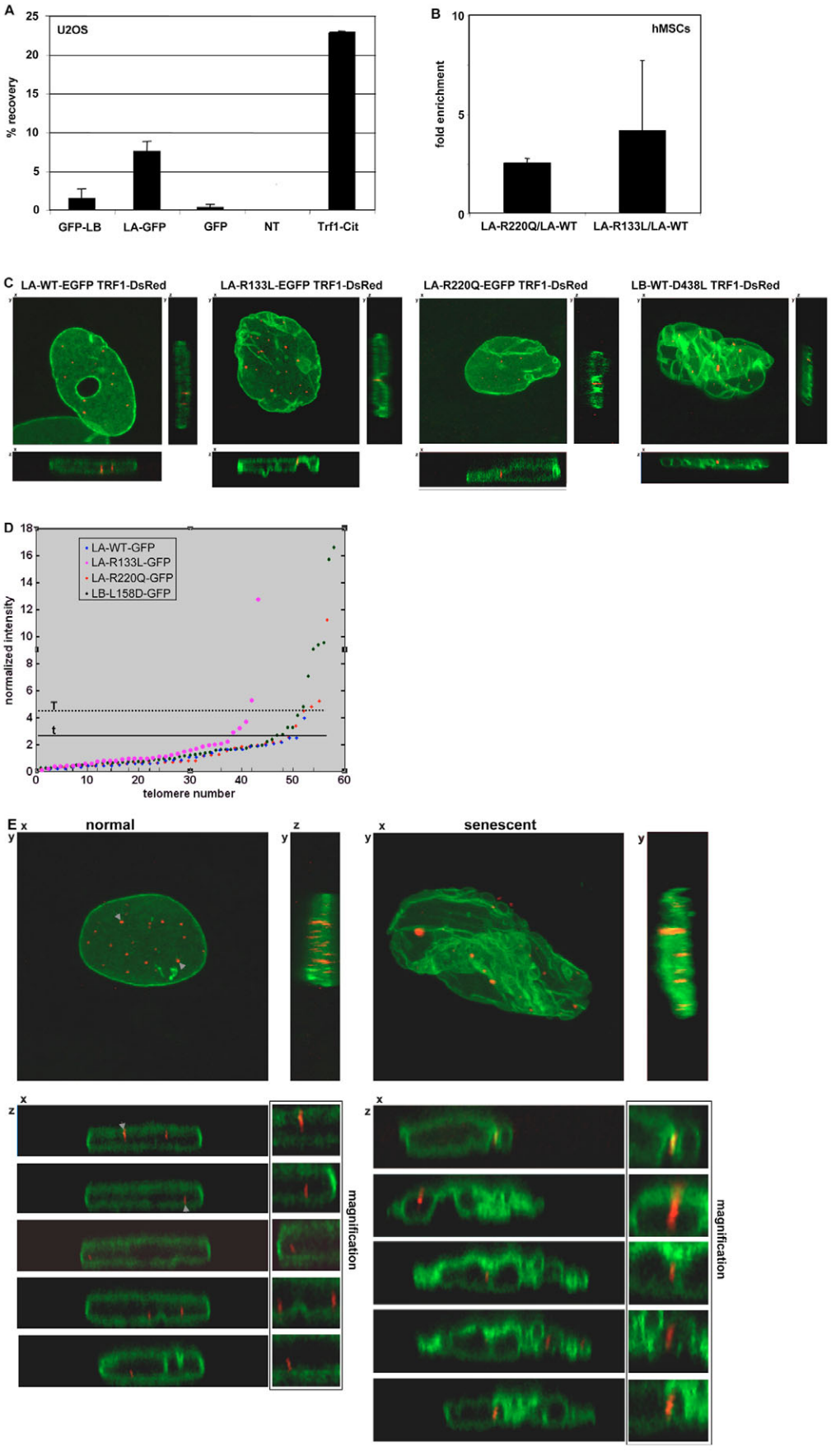


**Fig. 6.** Increase in telomere binding to lamina intranuclear structures. Telomeres bind to the nuclear lamina. (A) U2OS cells were transduced with lentiviral vectors that express the lamin B (LB)-WT or lamin A (LA)-WT fused to GFP. As controls, cells were transduced with CMV-GFP or TRF1-citrine lentiviral vectors, or were left nontransduced (NT). Cells were crosslinked with formaldehyde 2 days after transduction, and isolated chromatin was used for chromatin immunoprecipitation with antibodies against GFP. Purified DNA from the immunoprecipitations and input fractions were used for QPCR using telomere primers. Histograms show % recovery after normalization to data obtained from NT cells. Data represent the average of two independent experiments. (B) Enrichment of telomere binding to the nuclear lamina in cells expressing mutation in lamina genes. Human MSCs at passage 6 were transduced with the lentiviral vectors that express the lamin B(LB)-WT, lamin A (LA)-WT, LA-R133L, LA-R220Q or LB-L158D fused to EGFP. Five days after transduction, cells were crosslinked with formaldehyde, and isolated chromatin was used for chromatin immunoprecipitation (ChIP) with antibodies against GFP. Purified DNA from the immunoprecipitations and input fractions were used for QPCR using telomere-specific primers. Percentage recovery was normalized to data obtained from NT cells. Histograms show fold enrichment in % input LA-R133L or LA-R220Q over LA-WT, and LB-L158D over LB-WT. Averages represent two independent experiments. (C) Maximum projections of *x-y* axis taken from representative hMSCs at passage 5 expressing TRF1-DsRed together with LA-WT-EGFP, LA-R133L-EGFP, LA-R220Q-EGFP and LB-L158D-EGFP. Overlap between lamina intranuclear structures and telomere aggregates is shown in representative single cross-sections at the *x-z* and *y-z* axis. Quantification of telomere aggregates in hMSCs expressing the LA-R133L, LA-R220Q and LB-L158D mutants. (D) TRF1 fluorescent intensities were measured from confocal images taken from cells. Plots show the fluorescent intensities of TRF1-DsRed dots from representative cells expressing LA-WT (blue dots), LA-R133L (pink dots), LA-R220Q (red dots) and LB-L158D (green dots) fused to EGFP. The thresholds for calculation of small and large telomere aggregates are indicated with straight or dotted lines, respectively. (E) hMSCs at passage 6 were transduced with Lamin-B-EGFP (green) and the TRF1-DsRed (red) lentiviral vectors. Confocal images were taken from normal or senescent living cells at passage 8. 3D reconstructions were processed in TeloView, single sections on the *x-z* axis were produced in DipImage at equal intervals. The boxed images are a ×1.65 magnification of the *x-z* sections.

positive correlation between lamina intranuclear structures and the formation of telomere aggregates.

To investigate whether telomere aggregates are indeed associated with lamina intranuclear structures, confocal Z-stacks were taken from live cells at passage 8 expressing lamin-B-EGFP and TRF1-DsRed. Telomere aggregates were determined and marked using TeloView and the spatial localization was determined in cross-sections (Fig. 6E). A few telomeres (3-5%) showed spatial overlap with the nuclear lamina in cells with an ellipsoid shape (Fig. 6E, left panel). However, telomere aggregates were found in close association with lamina intranuclear structures (Fig. 6E, right panel). Interestingly, some of the telomere aggregates showed a complete overlap with lamina intranuclear structures (Fig. 6E). Also, in cells expressing TRF1 together with one of the lamin mutants, overlap was found in single cross-sections between TRF1 and lamina intranuclear structures (Fig. 6C). Together, our results suggest that the binding of telomeres to the nuclear lamina is associated with the formation of telomere aggregates.

## Discussion

Ex vivo, hMSCs show features of cell senescence after a few cell divisions. Understanding the process of senescence in hMSCs is important because of its impact on clinical applications. As we studied cell senescence in primary cells that senesce ex vivo without molecular or genetic manipulation, it was essential to clearly distinguish between senescent and non-senescent hMSCs. Senescent cells were therefore characterized using Hayflick senescence-associated factors and the spatial structure of the nuclear lamina. Interestingly, senescent hMSCs revealed changes in lamina distribution before the appearance of the senescence-associated markers. Therefore we used the spatial organization of the lamina to distinguish between non-senescent and senescent hMSCs. Changes in lamina organization have not only been associated with senescence but also with aging and premature aging syndromes (reviewed in Broers et al., 2006). Our studies here show that in hMSCs, changes in lamina organization are associated with ex vivo senescence.

Cell senescence is associated with changes in gene activity (Ben Porath and Weinberg, 2005; Dhe-Paganon et al., 2002), and positioning of genes at the nuclear lamina results in their transcriptional repression (Pickersgill et al., 2006; Reddy et al., 2008; Scaffidi and Misteli, 2008). Thus far, however, it has not been reported that specific heterochromatic chromosome regions associate with the nuclear lamina when cells senesce. We developed quantitative imaging tools to determine the spatial localization of centromeres and telomeres with respect to the lamina in the nucleus of hMSCs. We found that, together with changes in lamina structure, the spatial distribution of telomeres and centromeres changes towards a more peripheral localization. Moreover, a spatial overlap of lamina intranuclear structures with telomeres and centromeres was found in senescent hMSCs, suggesting that the preferred peripheral localization of these sequences is a consequence of their binding to the lamina. In support of this model, an enhanced binding of telomeres to the lamina proteins was found in cells expressing mutant forms, which exhibit a distorted lamina structure. Previous studies described a preferred peripheral localization of centromeres in cell-cycle-arrested cells, fully differentiated cells and apoptotic cells (Takai et al., 2003; Weierich et al., 2003; Solovei et al., 2004; Wiblin et al., 2005; Raz et al., 2006). Since changes in cellular function are associated with changes in gene activity, we speculate that the peripheral localization of telomeres and centromeres contributes to establishing, and possibly stabilizing, changes in gene activity.

Based on our mathematical analysis of telomere fluorescence intensities, we found that during cell senescence, telomeres form objects that are highly fluorescent, which were absent in normal cells. The presence of these objects is consistent with the organization of telomeres in large aggregates. In mammalian cells, the formation of telomere aggregates was previously described in Myc-activated cells and in caspase-8-activated cells (Chuang et al., 2004; Raz et al., 2006). The functional relevance of telomere aggregates is unclear. Previous work shows that after TRF2 inhibition, DNA-damage proteins associate with telomeres and render them damaged (Takai et al., 2003). Because we found that telomere aggregates overlap with the DNA-damage marker γ-H2AX, but not TERT, we suggest that telomere aggregates are composed of damaged telomeres. γ-H2AX DNA foci accumulate at sites of double-strand breaks (DSBs) after cell irradiation. However, since some γ-H2AX DNA foci are not associated with DSB-repair proteins, especially in cells exposed to environmental changes other than irradiation (McManus and Hendzel, 2005; Takahashi and Ohnishi, 2005; Huang et al., 2006), it is essential to determine the function of telomere aggregates, and whether they are sites for DSBs. In addition, it is not well understood how telomere aggregates are formed. Expression of mutant lamin genes led to a distorted lamina structure and the formation of telomere aggregates. A spatial overlap between telomere aggregates and lamin B intranuclear structures was also found in senescent cells or in cells expressing lamin mutants, suggesting that the formation of telomere aggregates in senescent cells is associated with binding of telomeres to the lamina. We suggest that telomere binding to lamina proteins is enhanced when the intranuclear lamina structures are formed during cell senescence. Since we found that changes in lamina spatial organization are initiated at earlier passages compared with the formation of telomere aggregates, we therefore suggest that changes in lamin organization precede telomere aggregation. Consistent with this model, we recently reported that an increase in lamina intranuclear structures leads to the formation of telomere aggregates in caspase-8-activated cells (Raz et al., 2006).

To conclude, we suggest that the nuclear lamina has a role not only in regulating the transcriptional activity of individual genes (Pickersgill et al., 2006; Reddy et al., 2008; Scaffidi and Misteli, 2008), but also in the spatial positioning of heterochromatic regions, as shown for telomeres and centromeres. The interactions of telomeres and centromeres with the nuclear lamina might have a structural effect on nuclear organization. Alternatively, binding of heterochromatic regions to the nuclear lamina might affect the expression of genes in *trans*.

## Materials and Methods

### Cell culture

Human mesenchymal stem cells (hMSCs) were isolated from bone marrow samples as described previously (Knaän-Shanzer et al., 2005). Samples 35y and 81y were obtained from a 35-year-old and 81-year-old donor, respectively (S. Knaän-Shanzer, Leiden University Medical Centre, Leiden, The Netherlands; personal communication). After two passages of cell propagation, cells were stored in liquid nitrogen, and for the experiments described we started at passages three or four. Cells were cultured in plastic culture dishes with DMEM, without Phenol Red and supplemented with 20% fetal bovine serum (FCS), 1% glutamine and 1% penicillin streptomycin (P/S); medium refreshment was every 3-4 days. In every passage, cells were plated at 60-70% confluence, and were subcultured when 90-100% confluence was reached. During cell culture, the cells were checked to maintain the expression of the cell-surface markers CD105, CD44, CD106, CD90 and HLA class I for several passages. A substantial reduction in the growth rate of the 35y cells was observed after passages 10 to 11, and of the 81y cells after six to seven passages. With increasing

numbr of cell passages, the capacity of HMSCs to differentiate into the adipogenic and osteogenic lineage was reduced. Experiments were done using cells from the 35-year-old donor unless indicated otherwise. Prior to imaging or immunocytochemistry, cells were seeded on glass dishes. No morphological or growth changes were observed when cells grew on glass for at least three passages.

### Lentiviruses: construction, production and transduction

The lentiviral vectors used in this work are the so-called self-inactivating (SIN) vectors (Carlotti et al., 2004). The fusion genes lamin-B-EGFP, lamin-A-EGFP, lamin-A-DsRed, CenpA-EGFP, TRF1-DsRed and Trf2-citrine were cloned in the pRRL lentiviral vector, as described previously (Carlotti et al., 2005; Raz et al., 2006). The viral production and the cell transduction procedures were as described previously (Carlotti et al., 2004). After transduction, cells were cultured for additional passages without any selection pressure and without losing the transduced genes. The expression pattern and localization of the fused proteins was similar to the expression pattern of the endogenous proteins as verified with immunocytochemistry.

### Mutants

Point mutations were generated by PCR using the QuikChange site-directed mutagenesis protocol (www.stratagene.com/manuals/200518.pdf). The pRRL-CMV-laminA-R133L/R220Q-GFP mutants were generated using the following primers: R133L-FW: cctgatagctgctcaggctc**g**gctgaaggacctggaggc; R133L-RV: cctgatagct-gctcaggctc**t**gctgaaggacctggaggc. R220Q-FW: gctgcgtgagaccaagc**a**gcgtcatgagacccgac; R220Q-RV: gtcgggtctcatgacgc**t**gcttggtctcacgcagg. The mutated nucleotides are indicated in bold. The LaminB-L158D-GFP has been previously described (Raz et al., 2006). All mutant cDNAs were verified by sequencing.

### Senescence-associated β-galactosidase assay

The protocol for SA-β-gal activity was modified from a previously described protocol (Dimri et al., 1995). Cells were washed once with PBS (pH 7.2) and fixed in 2% formaldehyde in PBS for 5 minutes. Incubation with the X-Gal solution was carried out for 3 hours at 37°C. For the combination of the SA-β-gal activity essay with immunocytochemistry, the incubation with X-Gal was followed by five washes in PBS and incubation with 1% Triton X-100 in PBS for 10 minutes. Cells were then incubated with antibodies as described (Raz et al., 2006).

### Immunofluorescence and western blotting

Immunofluorescence and western blot analysis was performed using rabbit- or mouse-anti-human lamin A (1:1000; Santa Cruz); rabbit-anti-hTRF2 (1:1000 Imgenex); mouse-anti-hPML 5E10 (1:10) (Stuurman et al., 1992), mouse-anti-human p16(INK4a) (1:10, kindly provided by G. Peters, London Research Institute, UK, and by A. G. Jochemsen, Leiden University Medical Center, Leiden, The Netherlands), mouse-anti-p53 (1:100, kindly provided by A. G. Jochemsen), mouse-anti-TERT (C-term) clone Y182 (1:200; Epitomics), and mouse-anti-γ-H2AX (1:100, Upstate Biotech). For immunofluorescence, cells were seeded on glass plates and fixed prior to antibody incubation as described (Raz et al., 2006). Incubations with primary antibody were followed with an appropriate secondary antibody conjugated to DEAC, Cy5 or Alexa Fluor 488 (Molecular Probes), as indicated in the figure legends. For western blot analysis, cell lysates were prepared from about 500,000 cells.

### PNA in situ hybridization

In situ hybridization with a telomere repeat PNA probe was performed as described (Molenaar et al., 2003) with a few modifications. The pepsin treatment was performed in 0.05% pepsin, 10 mM HCl for 7 minutes. Following the hybridization procedure, cells were incubated with the anti-lamin A antibody as indicated above. Finally, cells were mounted in Citifluor.

### Chromatin immunoprecipitation

For ChIP experiments, U2OS cells or hMSCs PS 5 were transduced with the following lentiviral vectors: CMV-GFP, CMV-LB-WT-GFP, CMV-LB-D438L-GFP, CMV-LA-WT, CMV-LA-R220Q-GFP, CMV-TRF1-citrine. Non-transduced cells were used as a control. Chromatin was isolated 2 and 4 days following lentiviral transduction of U2OS cells or hMSCs, respectively. For U2OS cells, LV transduction efficiency was always close to 100%. For hMSCs, the transduction efficiency was around 30-50%. Expression levels were evaluated by western blot analysis. Chromatin preparation and ChIP experiments were performed as described (Nelson et al., 2006). Immunoprecipitation was performed with rabbit-anti-GFP antibody (1:1000; Roche). Calculation of the percentage recovery was performed as described (http://www.superarray.com/Manual/ChIPqpcrmanual.pdf). Quantitative PCR on telomeric sequences was done as described (Cawthon, 2002), using the iCycler iQ Real-Time PCR Detection System (BioRad) and a SYBR-Green-based kit for quantitative PCR (iQ Supermix, Bio-Rad). Amplification products were analyzed by gel electrophoresis and by dissociation curve analysis. Results were quantified using a standard curve generated with serial dilutions of input DNA. All ChIP experiments were performed in duplicate.

### Microscopy and Image processing

Image stacks were collected using a Leica TCS/SP2 confocal microscope system equipped with a ×100/1.4 NA plan Apo objective. The spatial sampling distance for the Leica confocal system was $\Delta z$=163 nm/voxel in the axial direction and $\Delta x$=$\Delta y$=40 nm/voxel to 60 nm/voxel in the lateral direction. The varying sampling distance in the lateral direction was used to accommodate cells of varying sizes. For the analysis of colocalization between lamin B-EGFP and TRF1-DsRed (Fig. 7F) $\Delta z$=122 nm/voxel. All image processing and analysis were performed using MatLab and the toolbox DIP-image (van der Heijden et al., 2004) (http://www.qi.tnw.tudelft.nl/DIPlib). Serial cross-sections were made in DipImage. Some of the two-dimensional images were taken with a Zeiss Axiovert (model 135TV) fluorescence microscope equipped with a 100-W mercury arc lamp and a ×100/1.3 NA plan Apo objective.

### Quantitative image analyses

Quantitative image analysis of telomeres and centromeres was performed using the software package TeloView (Vermolen et al., 2005). The spatial localization of telomere and centromere fluorescence dots relative to the lamina was performed in a new algorithm the developed for the hMSCs (Vermolen et al., submitted). Profiles of fluorescence intensities were produced with the Leica confocal software, version 2.5.

### Calculating the spatial localization of nuclear probes

The spatial positions of centromeres and telomeres relative to the nuclear sphere were calculated using a newly developed algorithm (Vermolen et al., 2008). In brief, the nuclear sphere was segmented from the lamin A or lamin B GFP signal or a logarithm stretch on the TRF1 or CenpA fluorescence signal. After the logarithmic stretch, a threshold is defined by the Isodata algorithm, which highlights the background of the probe. The new threshold highlights nuclear shape from the cytosolic background. After segmentation, the radial positions of all signal dots were normalized from 0 to 1, where 0 is the center of the nucleus and 1 the edge. The normalization step allows the comparison of pooled data from several nuclei. The probability that a probe can be found within a certain distance from the center of the cell can be described by a probability distribution function whose estimate is given as: $F(r_{\text{norm}})$=(number of observations $\leq r_{\text{norm}}$)/(total number of observations).

This distribution is sometimes referred to as a cumulative distribution function (CDF) and was plotted against the normalized nuclear radius. The Kolmogorov-Smirnov test (KS test) was applied to these CDF plots in the MatLab statistics toolbox (The MathWorks, Natick, MA).

### Definition of telomere aggregates

The mathematical method used for defining telomere aggregates will be described elsewhere (unpublished results). In brief, aggregates were defined as outliers from the normal set of voxel intensities. Based upon intensity, we distinguish between three classes of telomere voxels: normal, small aggregates, and large aggregates. The last two are considered to be outliers. The outliers are determined by an iterative threshold process. Normal telomeres are defined as ($i<t$), small aggregates: ($t<i<T$), and large aggregates: ($i>T$). In the iteration, an increasing number of outliers is found until the number of outliers ($n$) is the same as the number of outliers given by a threshold $t=\mu + t_s \sigma$ where $\mu$ is the mean and $\sigma$ is the standard deviation of the normal intensities and $t_s$ is given by the Student's $t$-test distribution with $P$=0.01 and $N$–1 ($N$=number of normal intensities) degrees of freedom. The threshold $T$ is defined as $T \geq 2t$.

### Electron microscopy

Cells were fixed in 1.5% glutaraldehyde in 0.1 M cacodylate buffer for 1 hour at room temperature, post-fixed in 1% $OsO_4$ in the same buffer for 1 hour at 4°C, dehydrated in a graded ethanol series and embedded in Epon. Ultrathin sections were post-stained with uranyl acetate and lead citrate and viewed with a CM10 electron microscope at 80 kV (Philips, Eindhoven, The Netherlands).

We thank Shoshan Knaän-Shamzer, Ietje van der Velde and Martijn Rabelink (Laboratory for Virus and Stem Cell Biology, Leiden University Medical Center, The Netherlands) for supplying hMSCs, advice on their culturing and for lentivirus productions, respectively. We thank Yolanda Ramos for help with the ChIP experiments and data analysis; Françoise Carlotti, Haico van Attikum and the members of R. Dirk's group for fruitful discussions. This research is granted by the Cyttron program, grant number BSIK03036.

## References

**Amrichova, J., Lukasova, E., Kozubek, S. and Kozubek, M.** (2003). Nuclear and territorial topography of chromosome telomeres in human lymphocytes. *Exp. Cell Res.* **289**, 11-26.

**Baxter, M. A., Wynn, R. F., Jowitt, S. N., Wraith, J. E., Fairbairn, L. J. and Bellantuono, I.** (2004). Study of telomere length reveals rapid aging of human marrow stromal cells following *in vitro* expansion. *Stem Cells* **22**, 675-682.

**Ben Porath, I. and Weinberg, R. A.** (2005). The signals and pathways activating cellular senescence. *Int. J. Biochem. Cell Biol.* **37**, 961-976.
**Bonab, M., Alimoghaddam, K., Talebian, F., Ghaffari, S., Ghavamzadeh, A. and Nikbin, B.** (2006). Aging of mesenchymal stem cell *in vitro*. *BMC Cell Biol.* **7**, 14-21.
**Broers, J. L., Ramaekers, F. C., Bonne, G., Yaou, R. B. and Hutchison, C. J.** (2006). Nuclear lamins: laminopathies and their role in premature ageing. *Physiol. Rev.* **86**, 967-1008.
**Capell, B. C. and Collins, F. S.** (2006). Human laminopathies: nuclei gone genetically awry. *Nat. Rev. Genet.* **7**, 940-952.
**Carlotti, F., Bazuine, M., Kekarainen, T., Seppen, J., Pognonec, P., Maassen, J. A. and Hoeben, R. C.** (2004). Lentiviral vectors efficiently transduce quiescent mature 3T3-L1 adipocytes. *Mol. Ther.* **9**, 209-217.
**Carlotti, F., Zaldumbide, A., Martin, P., Boulukos, K. E., Hoeben, R. C. and Pognonec, P.** (2005). Development of an inducible suicide gene system based on human caspase 8. *Cancer Gene Ther.* **12**, 627-639.
**Cawthon, R. M.** (2002). Telomere measurement by quantitative PCR. *Nucleic Acids Res.* 30, e47.
**Chuang, T. C, Moshir, S., Garini, Y., Chuang, A. Y., Young, I. T., Vermolen, B., van den Doel, R., Mougey, V., Perrin, M., Braun, M., Kerr, P. D., Fest, T., Boukamp, P. and Mai, S.** (2004). The three-dimensional organization of telomeres in the nucleus of mammalian cells. *BMC. Biol.* **2**, 12-21.
**Collado, M., Blasco, M. A. and Serrano, M.** (2007). Cellular senescence in cancer and aging. *Cell* **130**, 223-233.
**Cowell, I. G., Sunter, N. J., Singh, P. B., Austin, C. A., Durkacz, B. W. and Tilby, M. J.** (2007). gammaH2AX Foci Form Preferentially in Euchromatin after Ionising-Radiation. *PLoS ONE* **2**, e1057.
**Cremer, T., Kupper, K., Dietzel, S. and Fakan, S.** (2004). Higher order chromatin architecture in the cell nucleus: on the way from structure to function. *Biol. Cell.* **96**, 555-567.
**Dhe-Paganon, S., Werner, E. D., Chi, Y. I. and Shoelson, S. E.** (2002). Structure of the globular tail of nuclear lamin. *J. Biol. Chem.* **277**, 17381-17384.
**Dimri, G. P., Lee, X. H., Basile, G., Acosta, M., Scott, C., Roskelley, C., Medrano, E. E., Linskens, M., Rubelj, I., Pereirasmith, O. et al.** (1995). A biomarker that identifies senescent human-cells in culture and in aging skin *in vivo*. *Proc. Natl. Acad. Sci. USA* **92**, 9363-9367.
**Gerson, S. L.** (1999). Mesenchymal stem cells: no longer second class marrow citizens. *Nat. Med.* **5**, 262-264.
**Gilchrist, S., Gilbert, N., Perry, P. and Bickmore, W. A.** (2004). Nuclear organization of centromeric domains is not perturbed by inhibition of histone deacetylases. *Chromosome. Res.* **12**, 505-516.
**Gruenbaum, Y., Margalit, A., Goldman, R. D., Shumaker, D. K. and Wilson, K. L.** (2005). The nuclear lamina comes of age. *Nat. Rev. Mol. Cell. Biol.* **6**, 21-31.
**Huang, S., Risques, R. A., Martin, G. M., Rabinovitch, P. S. and Oshima, J.** (2008). Accelerated telomere shortening and replicative senescence in human fibroblasts overexpressing mutant and wild-type lamin A. *Exp. Cell Res.* **314**, 82-91.
**Huang, X., Tanaka, T., Kurose, A., Traganos, F. and Darzynkiewicz, Z.** (2006). Constitutive histone H2AX phosphorylation on Ser-139 in cells untreated by genotoxic agents is cell-cycle phase specific and attenuated by scavenging reactive oxygen species. *Int. J. Oncol.* **29**, 495-502.
**Jacob, K. N., Baptista, F., dos Santos, H. G., Oshima, J., Agarwal, K. and Garg, A.** (2005). Phenotypic heterogeneity in body fat distribution in patients with atypical Werner's syndrome due to heterozygous Arg133Leu lamin A/C mutation. *J. Clin. Endocrinol. Metab.* **90**, 6699-6706.
**Knaan-Shanzer, S., van de Watering, M. J. M., van der Velde, I., Goncalves, M. A. F. V., Valerio, D. and de Vries, A. A. F.** (2005). Endowing human adenovirus serotype 5 vectors with fiber domains of species B greatly enhances gene transfer into human mesenchymal stem cells. *Stem Cells.* **23**, 1598-1607.
**Le Blanc, K. and Pittenger, M.** (2005). Mesenchymal stem cells: progress toward promise. *Cytotherapy* **7**, 36-45.
**Luderus, M. E., van Steensel, B., Chong, L., Sibon, O. C., Cremers, F. F. and de Lange, T.** (1996). Structure, subnuclear distribution, and nuclear matrix association of the mammalian telomeric complex. *J. Cell Biol.* **135**, 867-881.
**McManus, K. J. and Hendzel, M. J.** (2005). ATM-dependent DNA damage-independent mitotic phosphorylation of H2AX in normally growing mammalian cells. *Mol. Biol. Cell* **16**, 5013-5025.
**Molenaar, C., Wiesmeijer, K., Verwoerd, N. P., Khazen, S., Eils, R., Tanke, H. J. and Dirks, R. W.** (2003). Visualizing telomere dynamics in living mammalian cells using PNA probes. *EMBO J.* **22**, 6631-6641.
**Narita, M., Nunez, S., Heard, E., Narita, M., Lin, A. W., Hearn, S. A., Spector, D. L., Hannon, G. J. and Lowe, S. W.** (2003). Rb-mediated heterochromatin formation and silencing of E2F target genes during cellular senescence. *Cell* **113**, 703-716.
**Nelson, J. D., Denisenko, O. and Bomsztyk, K.** (2006). Protocol for the fast chromatin immunoprecipitation (ChIP) method. *Nat. Protoc.* **1**, 179-185.
**Parsch, D., Fellenberg, J., Brummendorf, T. H., Eschlbeck, A. M. and Richter, W.** (2004). Telomere length and telomerase activity during expansion and differentiation of human mesenchymal stem cells and chondrocytes. *J. Mol. Med.* **82**, 49-55.
**Pickersgill, H., Kalverda, B., de Wit, E., Talhout, W., Fornerod, M. and van Steensel, B.** (2006). Characterization of the Drosophila melanogaster genome at the nuclear lamina. *Nat. Genet.* **38**, 1005-1014.
**Pittenger, M. F., Mackay, A. M., Beck, S. C., Jaiswal, R. K., Douglas, R., Mosca, J. D., Moorman, M. A., Simonetti, D. W., Craig, S. and Marshak, D. R.** (1999). Multilineage potential of adult human mesenchymal stem cells. *Science* **284**, 143-147.
**Raz, V., Carlotti, F., Vermolen, B. J., van der Poel, E., Sloos, W. C. R., Knaan-Shanzer, S., de Vries, A. A. F., Hoeben, R. C., Young, I. T., Tanke, H. J. et al.** (2006). Changes in lamina structure are followed by spatial reorganization of heterochromatic regions in caspase-8-activated human mesenchymal stem cells. *J. Cell Sci.* **119**, 4247-4256.
**Reddy, K. L., Zullo, J. M., Bertolino, E. and Singh, H.** (2008). Transcriptional repression mediated by repositioning of genes to the nuclear lamina. *Nature* **45**, 243-247.
**Scaffidi, P. and Misteli, T.** (2006). Lamin A-dependent nuclear defects in human aging. *Science* **312**, 1059-1063.
**Scaffidi, P. and Misteli, T.** (2008). Lamin A-dependent misregulation of adult stem cells associated with accelerated ageing. *Nat. Cell Biol.* **10**, 452-459.
**Sedelnikova, O. A., Horikawa, I., Zimonjic, D. B., Popescu, N. C., Bonner, W. M. and Barrett, J. C.** (2004). Senescing human cells and ageing mice accumulate DNA lesions with unrepairable double-strand breaks. *Nat. Cell Biol.* **6**, 168-170.
**Sexton, T., Schober, H., Fraser, P. and Gasser, S. M.** (2007). Gene regulation through nuclear organization. *Nat. Struct. Mol. Biol.* **14**, 1049-1055.
**Shay, J. W. and Wright, W. E.** (2007). Hallmarks of telomeres in ageing research. *J. Pathol.* **211**, 114-123.
**Shibata, K. R., Aoyama, T., Shima, Y., Fukiage, K., Otsuka, S., Furu, M., Kohno, Y., Ito, K., Fujibayashi, S., Neo, M. et al.** (2007). Expression of the p16INK4A gene is associated closely with senescence of human mesenchymal stem cells and is potentially silenced by DNA methylation during *in vitro* expansion. *Stem Cells* **25**, 2371-2382.
**Shoeman, R. L. and Traub, P.** (1990). The *in vitro* DNA-binding properties of purified nuclear lamin proteins and vimentin. *J. Biol. Chem.* **265**, 9055-9061.
**Solovei, I., Schermelleh, L., During, K., Engelhardt, A., Stein, S., Cremer, C. and Cremer, T.** (2004). Differences in centromere positioning of cycling and postmitotic human cell types. *Chromosoma* **112**, 410-423.
**Stenderup, K., Justesen, J., Clausen, C. and Kassem, M.** (2003). Aging is associated with decreased maximal life span and accelerated senescence of bone marrow stromal cells. *Bone* **33**, 919-926.
**Strelkov, S. V., Herrmann, H. and Aebi, U.** (2003). Molecular architecture of intermediate filaments. *Bioessays* **25**, 243-251.
**Stuurman, N., de Graaf, A., Floore, A., Josso, A., Humbel, B., de Jong, L. and van Driel, R.** (1992). A monoclonal antibody recognizing nuclear matrix-associated nuclear bodies. *J. Cell Sci.* **101**, 773-784.
**Sugimoto, K., Fukuda, R. and Himeno, M.** (2000). Centromere/kinetochore localization of human centromere protein A (CENP-A) exogenously expressed as a fusion to green fluorescent protein. *Cell Struct. Funct.* **25**, 253-261.
**Taddei, A., Hediger, F., Neumann, F. R. and Gasser, S. M.** (2004). The function of nuclear architecture: a genetic approach. *Annu. Rev. Genet.* **38**, 305-345.
**Takahashi, A. and Ohnishi, T.** (2005). Does γH2AX foci formation depend on the presence of DNA double strand breaks? *Cancer Lett.* **229**, 171-179.
**Takai, H., Smogorzewska, A. and de Lange, T.** (2003). DNA damage foci at dysfunctional telomeres. *Curr. Biol.* **13**, 1549-1556.
**van der Heijden, F., Duin, P. R. W., de Ridder, D. and Tax, D. M. J.** (2004). *Classification, Parameter Estimation and State Estimation: An Engineering Approach Using Matlab*. Wiley.
**Vermolen, B. J., Garini, Y., Mai, S., Mougey, V., Fest, T., Chuang, T. C., Chuang, A. Y., Wark, L. and Young, I. T.** (2005). Characterizing the three-dimensional organization of telomeres. *Cytometry A* **67**, 144-150.
**Vermolen, B. J., Garini, Y., Young, I. T., Dirks, R. W. and Raz, V.** (2008). Segmentation and analysis of the three-dimensional redistribution of nuclear components in human mesenchymal stem cells. *Cytometry A* **73**, 816-824.
**Weierich, C., Brero, A., Stein, S., von Hase, J., Cremer, C., Cremer, T. and Solovei, I.** (2003). Three-dimensional arrangements of centromeres and telomeres in nuclei of human and murine lymphocytes. *Chromosome. Res.* **11**, 485-502.
**Wiblin, A. E., Cui, W., Clark, A. J. and Bickmore, W. A.** (2005). Distinctive nuclear organisation of centromeres and regions involved in pluripotency in human embryonic stem cells. *J. Cell Sci.* **118**, 3861-3868.
**Yan, P.** (2004). Immunohistochemical localization of hTERT protein in human tissues. *Histochem. Cell Biol.* **121**, 391-397.
**Zimmermann, S., Voss, M., Kaiser, S., Kapp, U., Waller, C. F. and Martens, U. M.** (2003). Lack of telomerase activity in human mesenchymal stem cells. *Leukemia* **1**, 1146-1149.